



Open Archive TOULOUSE Archive Ouverte (OATAO)

OATAO is an open access repository that collects the work of Toulouse researchers and makes it freely available over the web where possible.

This is an author-deposited version published in : <http://oatao.univ-toulouse.fr/>
Eprints ID : 15847

To link to this article : DOI : 10.1016/j.memsci.2016.03.058
URL : <http://dx.doi.org/10.1016/j.memsci.2016.03.058>

To cite this version : El Rayess, Youssef and Manon, Yannick and Jitariouk, Nicolas and Albasi, Claire and Mietton-Peuchot, Martine and Devatine, Audrey and Fillaudeau, Luc *Wine clarification with Rotating and Vibrating Filtration (RVF): Investigation of the impact of membrane material, wine composition and operating conditions.* (2016) Journal of Membrane Science, vol. 513. pp. 47-57. ISSN 0376-7388

Any correspondence concerning this service should be sent to the repository administrator: staff-oatao@listes-diff.inp-toulouse.fr

Wine clarification with Rotating and Vibrating Filtration (RVF): Investigation of the impact of membrane material, wine composition and operating conditions

Youssef El Rayess^{a,b,e,*}, Yannick Manon^c, Nicolas Jitariouk^d, Claire Albasi^b, Martine Mietton Peuchot^{f,g}, Audrey Devatine^{b,f,g}, Luc Fillaudeau^c

^a Faculty of Agricultural and Food Sciences, Holy Spirit University of Kaslik (USEK), Jounieh, Lebanon

^b Université de Toulouse, INPT, UPS, Laboratoire de Génie Chimique, 4 Allée Emile Monso, F31432 Toulouse, France

^c LISBP, Université de Toulouse, CNRS, INRA, INSA, 135 Avenue de Rangueil, F-31077 Toulouse, France

^d RVF Filtration, 92, rue du Moulin Vert, 75014 Paris, France

^e Centre de Viticulture et d'Enologie de Midi-Pyrénées, Avenue de l'Agrobiopôle, 31320 Castanet-Tolosan, France

^f Université de Bordeaux, ISVV, EA 4577, Unité de recherche OENOLOGIE, 33882 Villenave d'Ornon, France

^g INRA, ISVV, USC 1219 OENOLOGIE, 33882 Villenave d'Ornon, France

A B S T R A C T

For the first time in the literature, a shear enhanced process (or dynamic filtration) called Rotating and Vibrating Filtration (RVF technology) was investigated for wine clarification. The impact of membrane material (hydrophilic PES and hydrophobic PTFE with a cut-off of 0.2 μm), wine composition (filtered wine, FW and Crude simulated wine, CSW) and operating conditions (transmembrane pressure and rotational frequency) are reported.

RVF module is characterized by a complex hydrodynamic generated by a 3 flat blades impeller in a confined cell. An additional driving force is generated by rotational frequency and is taken into account to calculate the apparent and real permeabilities.

Filtered wine (FW) generates an irreversible fouling whatever hydrophilic or hydrophobic membrane material. Even if PES membranes performances ($L_{p0 \text{ final}} = 1670 \text{ L h}^{-1} \text{ m}^{-2} \text{ bar}^{-1}$) were higher compared to those of PTFE membranes ($L_{p0 \text{ final}} = 170 \text{ L h}^{-1} \text{ m}^{-2} \text{ bar}^{-1}$), nor rotational frequency (mechanical stress), nor water rinsing did significantly remove or reduce fouling but, on the contrary, favors its compression and membrane plugging.

Crude simulated wine (CSW) includes pectins, tannins and mannoproteins. CSW filtration runs demonstrated a mechanical impact onto fouling reduction with PES and PTFE membranes. However mechanical efficiency is moderated by material properties which generated irreversible fouling with different magnitudes. PTFE and PES permeability gains stand for +34% and +300% respectively. Finally, a "critical frequency" is defined above which a permeability increase and hydraulic resistance reduction is induced by rotational frequency (22 and 30 Hz for PES and PTFE membranes respectively).

Keywords:

Rotating and Vibrating Filtration
Wine clarification
Critical frequency
Dynamic filtration

1. Introduction

Cross-flow microfiltration (CFMF) is a membrane process largely implemented in wine cellars. Cross-flow microfiltration offers a number of additional advantages comparing to traditional processes such as elimination of filter aids use and its associated environmental problems, the combination of clarification, microbial stabilization and sterile filtration in one single continuous

operation as well as economic and operational benefits.

One of the major inhibiting factors for successful commercialization and development of cross-flow microfiltration in wine industry is membrane fouling. This latter results in the reduction of the flux to far below the theoretical capacity of the membrane. Fouling by wine constituents (especially polyphenols, polysaccharides, yeasts and bacteria) occurs gradually with filtration time and can take various forms, such as adsorption, pore blockage, deposition or gel formation [1,2].

There have been many attempts to reduce membrane fouling and enhance the permeate flux during the CFMF of wine [1]. Till now, a little is referenced in the literature concerning the control of membrane fouling by mechanical or chemical techniques in

* Corresponding author at: Faculty of Agricultural and Food Sciences, Holy Spirit University of Kaslik (USEK), Jounieh, Lebanon.

E-mail address: youssefrayess@usek.edu.lb (Y.E. Rayess).

enology. Critical flux can be a key parameter of the control of membrane fouling as it is depending at the same time on the hydrodynamics and physico-chemistry (membrane/solutes interactions). The attempts to determine a critical flux in wine micro-filtration have failed [3,4] in contrary to Bessiere et al. [5] who determined the critical conditions in water filtration. El Rayess et al. [4] introduced the concept of threshold flux to wine micro-filtration. From this concept, authors defined a new fouling criterion based on the ratio between irreversible resistance and hydraulic membrane resistance. This ratio may vary depending on the requirements of researchers and industrials.

In conventional cross-flow microfiltration, high fluid velocities are generally necessary to induce high shear rates at the membrane surface in order to limit the growth of cake on the membrane. But, it generates large axial pressure gradients. These high velocities and pressure gradients require energy and cause large pressure drops along the membrane leading to a non-optimal membrane utilization. To improve the efficiency of the filtration process and maintain the state of cleanliness of the membrane filtering surfaces at an acceptable level during the filtration process, most of commercial filtration devices are equipped with a reverse filtering system. Back-flushing, backwashing and back-pulsing are all methods of operation in which the transmembrane pressure is periodically inverted by the use of a secondary pump, so that permeate flows back into the feed, lifting the fouling layer from the surface of the membrane. These steps are time consuming and adding up mechanical stress to the filtration devices resulting in a loss of capacity and efficiency of the equipment. Also, these techniques seem to be inefficient within the first 15 min of filtration (in-situ observations on industrial equipment) depending on wine composition, treatments during winemaking and operating conditions of filtration.

Another strategy in the reduction of membrane fouling is the introduction of dynamic filtration in wine industry. The principle of the dynamic filtration consists in creating a high shear rate at the membrane surface. The high shear rate can be obtained by rotating or vibrating the membrane, by a disk rotating near a fixed circular membrane or by the action of an agitator near a fixed membrane [6]. One of the advantages of this filtration is that it permits to decouple the inlet flow-rate into the module from membrane shear rate [7]. It also allows working with low transmembrane pressures.

During the last 15 years, dynamic filtration systems have been developed and studied for applications in food (milk, cheese, beer and fruit juices) and biotechnological industries [8–16]. Nowadays, no scientific research has been conducted on dynamic filtration for the clarification of wine. In the wine industry, TMCI Padovan introduced the first rotating dynamic crossflow filter (Dynamos[®]). In the literature, the system used by this company is known as multi-shafts systems with rotating ceramic membranes and was developed and commercialized many years ago [17]. This system consists into two stacks of rotating membranes. The two shafts rotate countercurrent in order to create the maximum shear forces at the membrane surface.

Although clarification of wine by conventional membrane technologies has been widely investigated and reviewed [1], the originality of this paper is the study for the first time of a shear enhanced process (RVF) for wine clarification. The objectives of this study are: (i) to investigate the feasibility of the RVF technology (Rotating and Vibrating Filtration technology) in wine clarification, (ii) to test different membrane materials (PES and PTFE for their respective hydrophilic and hydrophobic properties), (iii) to test the impact of wine composition on filtration performances, and (iv) to optimize the operating conditions of the RVF.

2. Theory

Theoretical analysis and literature survey highlight that the local shear rate could not be easily estimated in the RVF module. The investigation of hydrodynamic behaviour is required to understand and model local phenomena, but the whole difficulty rests in the complex hydrodynamics of the RVF system. In previous publication [13], the friction and the power consumption curves in the RVF module (Fig. 1) were reported. A semi-empirical correlation has been established to integrate the impact of the rotating speed on friction factor [18]. The additional pressure in the filtration room is reported and is given by Bernoulli's equation. It affords the core velocity coefficient between the impeller (agitator) and the membranes.

2.1. Core velocity coefficient and radial pressure induced by mixing

According to Darcy's law, permeate flux (J) is calculated by Eq. (1):

$$J = \frac{Q_p}{S} = \frac{\Delta P}{\mu_p \cdot Rh} = L_p \cdot \Delta P \quad \text{with} \quad \Delta P = (PR_m + PR_{Out})/2 - PP \quad (1)$$

where J is flux [m s^{-1}], Q_p permeate flow-rate [$\text{m}^3 \text{s}^{-1}$], S membrane area [m^2], ΔP the transmembrane pressure [Pa], μ_p the permeate viscosity [Pa s], Rh the total hydraulic resistance [m^{-1}], L_p the permeability [$\text{m s}^{-1} \text{Pa}^{-1}$], PR_m , PR_{Out} and PP respectively inlet, outlet and permeate relative pressures [Pa].

Bouzerar et al. [19,20] investigated the internal fluid mechanics of the system with stationary membrane and rotating disk. They showed that the boundary layers developing on the rotating and on the stationary discs have different thickness due to a radial outward flow generated by the centrifugal forces. The boundary layers are separated by an inviscid fluid core which rotates at an angular velocity ($k \cdot 2 \cdot \pi \cdot N$) with a core velocity coefficient (k) inferior to 1 and N the rotational frequency [Hz]. The core velocity coefficient depends on disk geometry and the distance membrane/disk [20,21]. The radial pressure gradient in the boundary layer is equal to that in the inviscid core and is given by (Eqs. (2) and 3):

$$\frac{\partial p}{\partial r} = \rho \cdot r \cdot (k \cdot 2 \cdot \pi \cdot N)^2 \quad (2)$$

$$p(r) = p_0 + \rho \cdot g \cdot z(r) + 2 \cdot \rho \cdot (k \cdot \pi \cdot N)^2 \cdot r^2 \quad (3)$$

where ρ is the density [kg m^{-3}], p the pressure [Pa] and r the radius [m].

The integration of Eq. (3) allows the calculation of the pressure field. When the integration is divided by the membrane area from r_0 to r_{max} , it allows the determination of the mean additional pressure. The action of the impeller induces high local perturbations due to rotational frequency (N) and pressure fluctuation. Fillaudeau et al. [13] determined the local additional pressure ΔP_{ag} by measuring the flux versus the radial position and the rotational frequency (Fig. 2). The permeate flux is given by Eq. (4) and depends on the rotation frequency and the radial position.

$$J(0, r \text{ to } r + dr) = \frac{\Delta P}{\mu_p \cdot Rh_m}$$

$$J(N, r \text{ to } r + dr) = \frac{(\Delta P + \Delta P_{ag}(N, r))}{\mu_p \cdot Rh_m} \quad (4)$$

where Rh_m is specifically the hydraulic resistance of clean membrane [m^{-1}].

The additional pressure in the filtration module is given by

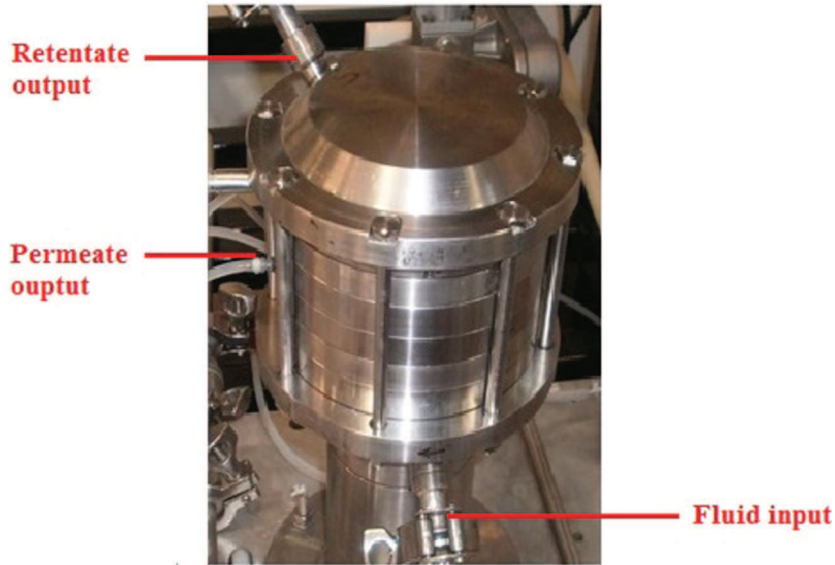
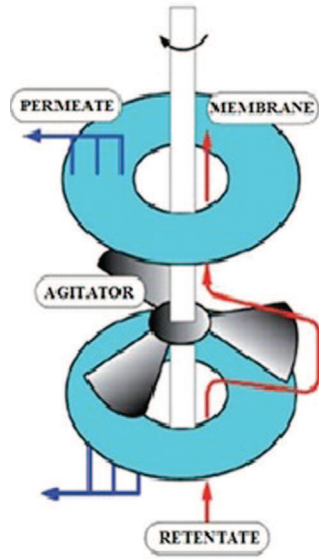


Fig. 1. Scheme and illustration of the Rotating and Vibrating Filtration module.

Bernoulli's equation and permit to determine the core velocity coefficient (k) between the impeller and the membrane. The core velocity coefficient does not vary too much with radial position. The effect of the impeller velocity on the local additional pressure ΔP_{ag} was described by Eq. (5), with $k=0.62$ ($R^2=0.994$), $r_0=25$ mm, $r_{max}=68$ mm and $0 < N < 50$ Hz.

$$\Delta P_{ag}(N, r) = p(r) - TMP = 2 \cdot \rho \cdot (k \cdot \pi \cdot N)^2 \cdot r^2 \quad (5)$$

where TMP is the efficient driving force [Pa].

2.2. "Apparent" and "real" permeability

The average permeability can be calculated according to Darcy's law considering two driving forces: (i) the conventional transmembrane pressure considering the filtration module and taking into account inlet and outlet retentate pressure and permeate pressure; (ii) the transmembrane pressure and the average additional mixing pressure within the filtration compartments. Both definitions will be respectively named apparent (Eq. (6)) and real permeabilities (Eq. (7)).

$$\bar{J} = \frac{Q_p}{S} = \frac{\Delta P}{\mu_p \cdot Rh} = Lp_{\text{Apparent}} \cdot \Delta P \quad (6)$$

$$\bar{J} = \frac{Q_p}{S} = \frac{(\Delta P + \Delta \bar{P}_{ag})}{\mu_p \cdot Rh} = Lp_{\text{Real}} \cdot (\Delta P + \Delta \bar{P}_{ag}) \quad (7)$$

Even if the conventional transmembrane pressure (ΔP) is used as reference; the local and mean additional pressure and flux could be calculated knowing the additional mixing pressure (Eq. (8)):

$$\Delta \bar{P}_{ag} = \frac{1}{S(r_{Max}) - S(r_0)} \iint_S \Delta P_{ag}(N, r) \cdot dS \Rightarrow \Delta \bar{P}_{ag} = \rho \cdot (k \cdot N \cdot \pi)^2 \cdot (r_{Max}^2 + r_0^2) \quad (8)$$

3. Material and methods

3.1. Experimental set-up and instrumentation

The experimental set-up consisted of a 20 L recirculation tank (Chemap-Fermenter, Chemap AG, CH-8601 Volketswil), a displacement

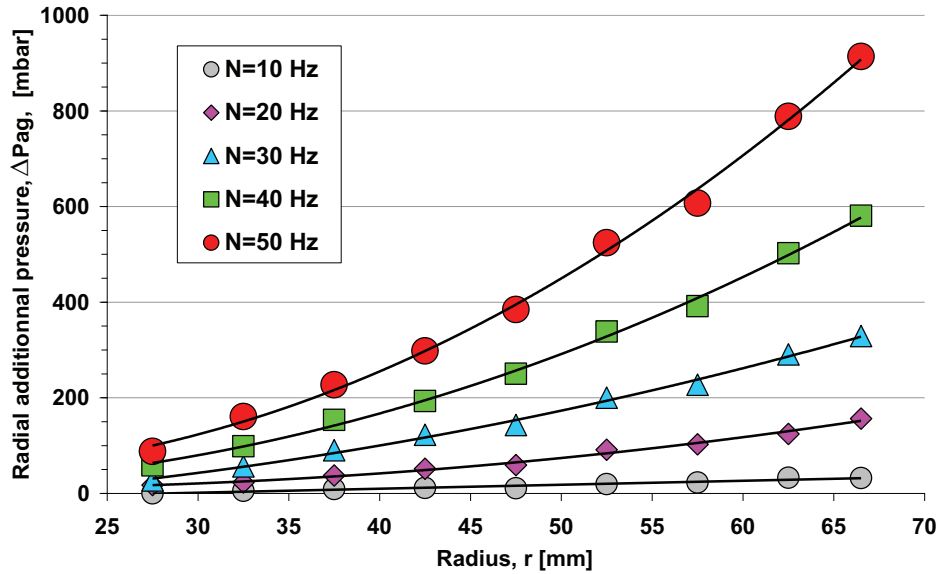


Fig. 2. Evolution of radial pressure distribution ΔP_{ag} versus radius and rotational frequency [13].

pump (TUTHILL DSG 1.3EET, Q_{max} : 350 L h⁻¹, P_{max} : 5 bar) and a fully instrumented derivation loop (Fig. 3). The RVF module is integrated into the derivation loop. The tank consisted in a cylindrical transparent vessel ($h=480$ mm, $D_v=250$ mm) equipped with three Rushton turbines ($D_a=80$ mm, four blades $w_a=l_a=20$ mm) and baffle basket ($nb=4$, $H_b=300$ mm, $w_b=30$ mm and a 170 mm diameter ring). Regulation loops enabled to control temperature, pH and dissolved oxygen. The permeate flow-rate was measured through weight balance (Sartorius CPA5201, 5200 g \pm 0.1).

The inlet of the derivation loop is located at the tank bottom in an external radial position. Experimental measurements along the derivation loop were performed on: relative and differential pressures, mass flow-rate, temperature, specific density, pH, dissolved oxygen and electrical conductivity. The relative pressure (BOURBON-HAENNI E913 33 B22 n°6008, \pm 0.2% full scale) was measured at pump outlet. A Coriolis Effect flow-meter (KROHNE, type MFS-7050-S06) enabled mass flow-rate (accuracy \pm 0.1% for a liquid and \pm 0.5% for a gas), temperature (precision \pm 1 °C) and specific density (precision \pm 2 kg m⁻³) measurements. The differential pressure (HONEYWELL - STD 120 n°0630-C2856562001001 and n°0630-C2856562001002, precision \pm 0.003% for 105 Pa in full scale) was used to determine the transmembrane pressure at the outlet of RVF module. pH was measured with a specific sensor (pH: Easyferm Plus VP/120-238 633, precision \pm 0.1). Finally, temperature was controlled by a platinum resistance probes (Pt 1000 Ω - IEC 751 - Class A).

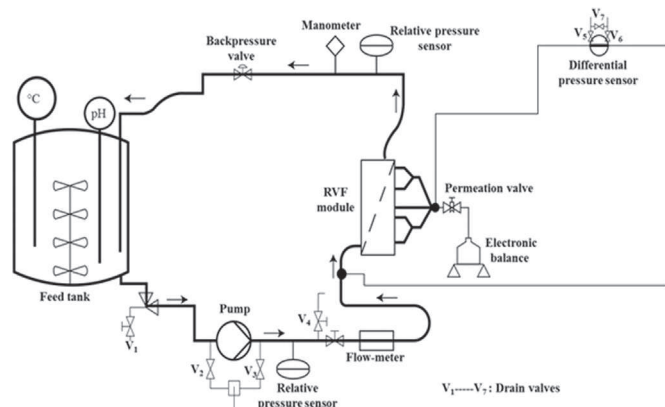


Fig. 3. Experimental set-up of the studied dynamic filtration module.

The experimental set-up was supervised with home-made software, LoCoPREL enabling (i) on-line acquisition of all sensors, (ii) the control of operating conditions and strategy (TMP, retentate flow-rate,...), (iii) the management of sampling, (iv) the control/command of derivation loop dedicated to filtration and physical measurements and (v) the simultaneous analyze of performances through calculated parameters (mass balance). A specific pump command was developed to monitor the flow-rate within the derivation loop. Two working modes were used: (i) constant flow-rate and (ii) flow-rate sequences. All electrical signals of sensors were conditioned using a data acquisition system (Agilent technologies, Loveland, USA, 34901A) including a multiplexer acquisition module (34901A) and a control command card (34907A) via a RS-232 liaison.

3.2. RVF module

The RVF laboratory module (filtration area 5.02×10^{-2} m²) is divided into two cells in series (estimated volume = 0.2 L cell⁻¹). Each cells contains two flat disc membranes fixed onto porous substrates which drain the permeate, and an impeller-shaped rotating body attached to a central shaft (Fig. 1). The membranes are mounted on the porous discs by fixing rings on the center and the circumference of the membranes. The fluid/retentate flows along the central shaft (inlet and outlet of each cell) and is distributed into the cell due to mixing effect. This simple mechanical device runs continuously and maintains a high shear rate as well as a hydrodynamic perturbation at the membrane surface. The impeller is made of three blades ($\varnothing_{ext}=142$ mm, thickness = 8 mm) included in a horizontal plane between two membranes. The dimensions of cell housing are 14 mm in height and 143 mm in diameter. The gap between the blade and the membrane is small and equal to 3 mm. Transmembrane pressure (up to 300 kPa) and rotational frequency (up to 50 Hz) can be adjusted to reach the optimal conditions for filtration. The two separated cells make it possible to work with two different membranes in similar conditions.

3.3. Membrane specifications

The membranes were flat discs with an external diameter of 142 mm. Filtration area per membrane is equal to 1.26×10^{-2} m² and forms a crown shape with an internal diameter of 50 mm and

an external diameter of 136 mm (including corrections due to the gasket). Membranes (cut-off: 0.2 μm) were respectively hydrophilic polyethersulfone (PES, Pall, Supor[®]-200-6654) and hydrophobic polytetrafluoroethylene (PTFE, Pall, TF-66145). Manufacturer specifications for PES membrane indicate a typical water permeability of $6.2 \times 10^{-8} \text{ m s}^{-1} \text{ Pa}^{-1}$ ($2.23 \times 10^4 \text{ L h}^{-1} \text{ m}^{-2} \text{ bar}^{-1}$) and a minimum bubble point (water) of 350 kPa. For PTFE membrane, the typical air permeability is $476 \times 10^{-8} \text{ m s}^{-1} \text{ Pa}^{-1}$ ($171 \times 10^4 \text{ L h}^{-1} \text{ m}^{-2} \text{ bar}^{-1}$, no data for water permeability) with a minimum bubble point at 100 kPa and a water breakthrough at 280 kPa.

The determination of hydrodynamic performances (permeability) was carried out with osmotic water. Due to their hydrophobic character, PTFE membranes were soaked for 24 h in a hydro-alcoholic solution (mixing ratio 5/95 v/v) in order to make it more water-permeable at low pressures. To notice that PTFE membranes are tested for the first time in wine clarification. According to literature, no attempts were made in wine filtration using PTFE membranes.

3.4. Experimental fluids

The choice of experimental fluids composition in this study is based on studies made on red wine CFMF by El Rayess et al. [2,4]. Its main characteristics are a 12% v/v ethanol, pH equal to 3.6, a total acidity equal to 3.48 and 2.43 g/L (eq. H_2SO_4) before and after stabilization respectively. The Filtered Wine (FW) is a wine clarified on ceramic membrane (0.2 μm); it is used to analyze the impact of wine molecules adsorption on membrane materials because the wine is free from particles and big colloids. The Crude Simulated Wine (CSW) is used to imitate a crude wine. The CSW consists into FW loaded with 1.25 g L^{-1} of tannins, 0.25 g L^{-1} of pectins and 0.1 g L^{-1} of mannoproteins. It is used to analyze the fouling mechanisms by this wine during RVF filtration.

3.4.1. Red wine

The red wine used in the present study was elaborated two years ago at the cooperative cellar of Rabastens from Duras, Fer Servadou and Syrah grape varieties. Thermo-*vinification* process was used to elaborate this wine in order to increase the extraction of polyphenolic compounds. After alcoholic and malo-lactic fermentations, the wine was centrifuged at the cellar in order to remove microorganisms and particles. A filtration was performed in a cross-flow microfiltration pilot plant using organic membrane with a pore size of 0.2 μm before storing at the cellar. In the lab, the wine is stored at 4 °C. Before experiments, a second cross-flow microfiltration (cut-off: 0.2 μm) is performed in order to eliminate potassium tartrate crystals, precipitates and microorganisms. This final step allows obtaining the filtered wine (FW) which is analyzed (chemical composition, physico-chemical properties).

3.4.2. Chemicals

The concentrations of added molecules are chosen according to those found in wine and identified in the literature [22]. Tannins (Biotan[®]) were purchased from Laffort (Bordeaux, France). These tannins are proanthocyanidic tannins extracted from grape skin with instantaneous dissolving. They were added to the wine (FW) with the concentration of 1.25 g L^{-1} . Pectin was purchased from Sigma-Aldrich (Lyon, France) and used at a concentration of 0.25 g L^{-1} . Mannoproteins (Mannostab[®]) were purchased from Laffort and added to the wine at a concentration of 0.1 g L^{-1} . Such composition is expected to mitigate crude wine and lead to identify fouling propensity and mechanism in comparison with FW filtration runs.

3.4.3. Wine components analysis

Turbidity indicates the presence of haze generated by macromolecules and particles in suspension. Measurements were

performed with a turbidimeter (Eutech Instrument, Singapore, model TN-100, range: 0-1000 NTU $\pm 2\%$) and expressed in Nephelometric Turbidity Unit (NTU). It corresponds to diffused light at 90°. Calibration is realised with standard solution at 0.2, 2, 80 and 200 NTU.

Spectrophotometric analyses were carried out on an Agilent 8453 UV/VIS spectrophotometer to determine the total polyphenol concentration and color intensity. Total polyphenols in wine were estimated by the Total Polyphenol Index (TPI, Eq. (9)) using the absorbance at 280 nm and under 1 cm optical path. Wine was diluted 100 times and measurement realised with special cells.

Color Intensity (CI, Eq. (10)) is the sum of optical densities (relatively to distillate water) at 420 nm (red color), 520 nm (yellow color) under 1 mm optical path.

Wine viscosity (μ) is determined with a controlled-stress rheometer (TA Instrument, model AR-2000ex). Geometry is a double gap Couette mobile (Dint1/2=40/40.76 mm and D3/4=43.92/44.92 mm, height=59.50 mm, sample volume=6 mL). Measurement were performed at 20 °C, with 20 increasing shear stress step between 1 and 300 s^{-1} (log scale).

$$\text{TPI} = \text{OD}_{280} \times \text{Dilution rate} \quad (9)$$

$$\text{CI} = \text{OD}_{420} + \text{OD}_{520} \quad (10)$$

$$\text{TMP} = \Delta P + \Delta P_{\text{ag}} \quad (11)$$

3.5. Filtration procedures

Two experimental campaigns were carried on the RVF filtration. Each is related to the type of the membrane and the operating procedure in which $\text{TMP} = \Delta P + \Delta P_{\text{ag}}$ (Eq. (11)). The experiments were conducted with 20 L of FW or CSW at 20 °C with a constant volume reduction ratio (VRR=1) indicating that permeate was return into tank product. The steps of these two experimental campaigns are summarized in Table 1. The frequency of 50 Hz is not used in this study due to periodic intensive retro-filtration. The maximum mixing rate is limited to 40 Hz under $\Delta P = 300 \text{ mbar}$.

4. Results and discussion

4.1. Overview of experiment up to qualitative performances

An overview of RVF filtration run with PTFE membrane is presented in Fig. 4. The permeability of PTFE membranes, flow-rate, pH, conductivity and ΔP are plotted as a function of time during the RVF filtration of filtered wine (FW) and crude simulated wine (CSW). Along all experiments, operating conditions (flow-rate, temperature, TMP) are perfectly controlled.

According to Darcy's law, water permeate flux (J) is calculated by Eq. (1). When the rotational frequencies are applied, the impeller induced significant local perturbations on the membrane surface due to the rotational frequencies and the local pressure fluctuation. Fillaudeau et al. measured the additional local pressure induced by the impeller rotational frequencies in terms of the radial position. Data presented in Table 2 are the average additional pressures ($\Delta P_{\text{ag}}^{\text{p}}$) given by Eq. (8) in terms of rotational frequencies and the real transmembrane pressure (TMP) which is the summation of ΔP and $\Delta P_{\text{ag}}^{\text{p}}$. The ratio $(\Delta P + \Delta P_{\text{ag}}^{\text{p}})/\Delta P$ demonstrates that above 10 Hz, the contribution of mixing, $\Delta P_{\text{ag}}^{\text{p}}$, could not be neglected into the transmembrane pressure driving force.

Water permeability of the membranes was realised using osmotic water with a mass flow-rate of 200 L h^{-1} . The real water

Table 1
Sequences and operating conditions of the RVF filtration experiments on FW and CSW with 0.2 μm PTFE and PES membranes.

Step	PES	PTFE
1	Determination of membrane initial permeability with osmotic water	Determination of membrane initial permeability with osmotic water
2	Filtration of FW $\Delta P=550$ mbar (N: 0, 10 and 20 Hz)	Filtration of FW $\Delta P=530$ mbar (N: 0, 10, 20 and 40 Hz)
3	Rinsing the pilot with tap water	Rinsing the pilot with tap water
4	Check water permeability of membranes with osmotic water	Check water permeability of membranes with osmotic water
5	Filtration of CSW $\Delta P=900$ mbar (N: 0, 10, 20, 30 and 40 Hz during 30 min) with intermediate return to 0 Hz during 30 min	Filtration of CSW $\Delta P=550$ mbar (N: 0, 10, 20, 30 and 40 Hz during 30 min) with intermediate return to 0 Hz during 30 min
6	Filtration of CSW at fixed N (40 Hz) and variable transmembrane pressure ($\Delta P=845, 607$ and 413 mbar during 1 h)	

permeabilities (calculated by (Eqs. (7) and (8))) were $4700 \text{ L h}^{-1} \text{ m}^{-2} \text{ bar}^{-1}$ ($130 \times 10^{-10} \text{ m s}^{-1} \text{ Pa}^{-1}$) for PES membrane and $2570 \text{ L h}^{-1} \text{ m}^{-2} \text{ bar}^{-1}$ ($71 \times 10^{-10} \text{ m s}^{-1} \text{ Pa}^{-1}$) for PTFE membrane. Permeability of PES membrane is in agreement with manufacturer specification. Considering the accurate driving force, none deviation in water permeability was observed for both membranes with the application of the rotational frequencies.

As expected results, the sharp decreases of permeability are observed between FW and CSW in addition to initial decrease (beginning of filtration with a defined product). The ratio of magnitude orders between water and FW permeabilities with PTFE membrane is around 10 with 2570 and $250 \text{ L h}^{-1} \text{ m}^{-2} \text{ bar}^{-1}$ respectively. The same ratio is observed between FW and CSW permeabilities with 250 and $25 \text{ L h}^{-1} \text{ m}^{-2} \text{ bar}^{-1}$. Due to higher FW permeabilities (generating high flux $> 1500 \text{ L h}^{-1} \text{ m}^{-2}$), the impact of rotational frequency appears limited and the added value by RVF seems to be not justified. On the opposite for CSW, a significant gain of flux (up to $+360\%$) induced by rotational frequency is observed and will be furtherly discussed in next part. With PES membrane, a similar behaviour maybe described.

Along FW and CSW filtrations, none significant deviation of the physico-chemical properties of retentate (pH, electrical conductivity, density) were observed. Table 3 reports the mean physico-chemical properties of permeate with FW and CSW along filtration whatever operating conditions. Analytical measurements carried out on samples from feed and permeate showed no significant difference between the 2 types of membranes in terms of compounds loss, especially the polyphenols. These latter are

Table 2
Apparent (ΔP) and real ($\Delta P + \Delta \bar{P}_{ag}$) transmembrane pressure (driving force) considering mixing effect in RVF module.

Rotation frequency [Hz]	ΔP [mbar]	$\Delta \bar{P}_{ag}$ [mbar]	TMP= $(\Delta P + \Delta \bar{P}_{ag})$ [mbar]	Ratio $(\Delta P + \Delta \bar{P}_{ag})/\Delta P$ []
0	300	0	300	1
10	300	19.02	319.02	1.02
20	300	76.11	376.11	1.26
30	300	171.25	471.25	1.57
40	300	304.40	604.40	2.01

represented by the CI and TPI parameters. The turbidity (NTU) is always inferior to 2 NTU for both mode of filtration which means that wines are perfectly limpid and brilliant.

4.2. RVF filtration of FW

The evolution of PES and PTFE membrane permeabilities are reported in Fig. 5 as a function of filtered volume and mixing rates in order to evaluate performances. Initial permeabilities, L_{p0} initial were $3817 \text{ L h}^{-1} \text{ m}^{-2} \text{ bar}^{-1}$ and $3750 \text{ L h}^{-1} \text{ m}^{-2} \text{ bar}^{-1}$ in comparison with water permeability equal to $4700 \text{ L h}^{-1} \text{ m}^{-2} \text{ bar}^{-1}$ and $2573 \text{ L h}^{-1} \text{ m}^{-2} \text{ bar}^{-1}$ respectively for PES and PTFE membranes (Table 4). Permeability increase with PTFE membranes was expected as FW contain almost 12% v/v ethanol.

Even if the initial water permeabilities of both membranes are

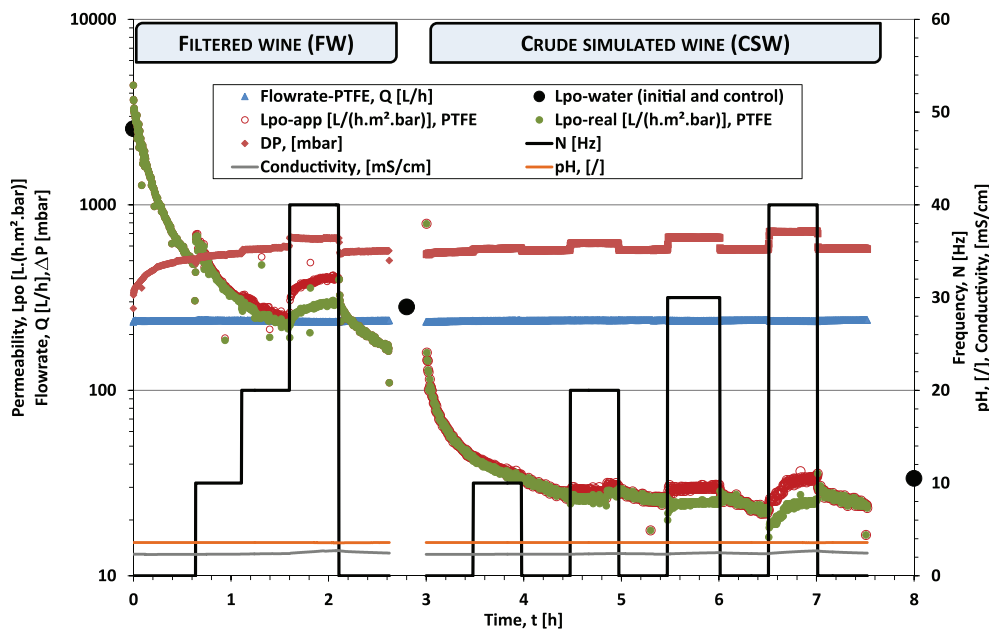


Fig. 4. Overview of RVF filtration run with PTFE membrane. Evolution of permeability of PTFE membranes, flow-rate, pH, conductivity and ΔP as a function of time during the RVF filtration of filtered wine (FW) and crude simulated wine (CSW) with RVF module.

Table 3

Physico-chemical properties of retentate and permeate during RVF filtration with 0.2 μm PES and PTFE membranes (mean values with standard deviation < 10%).

Membrane	Product	Retentate					Permeate		
		Conductivity [mS/cm]	pH [/]	Turbidity [NTU]	TPI [/]	CI [/]	Turbidity [NTU]	TPI [/]	CI [/]
PES	FW	2.15	3.53	0.1	44.2	0.84	0.1	44.0	0.83
	CSW	2.45	3.52	57	59.5	0.95	0.95	56.4	0.92
PTFE	FW	2.11	3.58	0.1	44.2	0.84	nr	nr	nr
	CSW	2.40	3.58	57	59.5	0.95	0.80	57.2	0.92

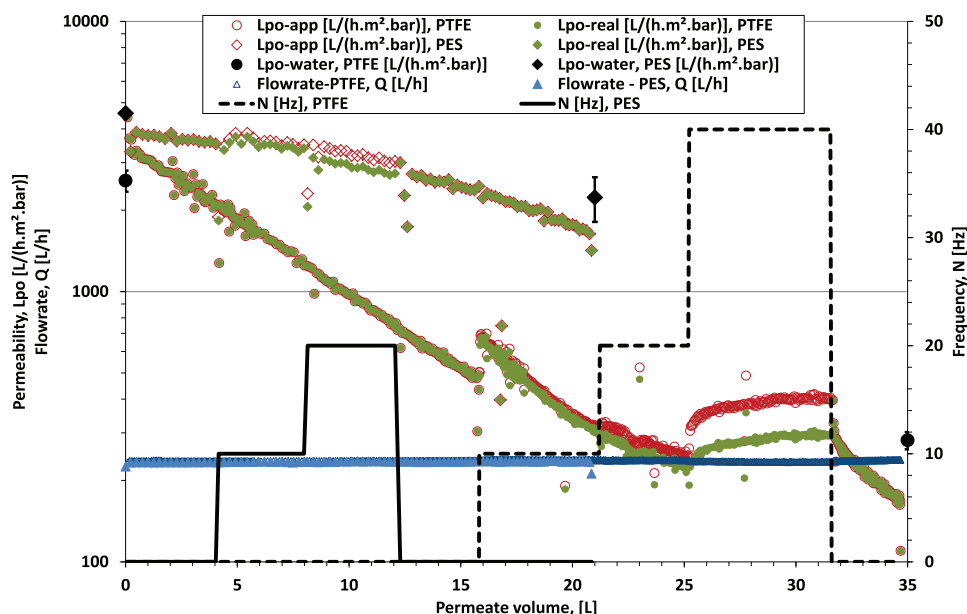


Fig. 5. Evolution of PES and PTFE membranes permeabilities as a function of permeate volume during the RVF filtration ($\Delta P \sim 550$ mbar, $N = 0, 10, 20$ and 40 Hz) of filtered wine (FW) with RVF module.

of the same order of magnitude, the permeabilities were divided by 2.3 after filtration of 20 FW liters with PES membranes and by 22 after filtration of 35 FW liters with PTFE membranes.

PES membrane permeabilities, L_{p0} final evolves down to $1676 \text{ L h}^{-1} \text{ m}^{-2} \text{ bar}^{-1}$. The application of rotational frequencies (10 Hz and 20 Hz) did not have any positive effect on the quantitative performances (constant decline of permeability despite mixing). This observation sustains the hypothesis of an irreversible fouling.

A net decrease of permeability is also observed for the PTFE membranes down to L_{p0} final = $170 \text{ L h}^{-1} \text{ m}^{-2} \text{ bar}^{-1}$ even if a moderate jump of permeability is identified for the rotational frequency at 40 Hz. This latter is due to a mechanical effect inducing a weak defouling. A sharp decrease in permeability is

observed after stopping the agitation clearly showing a fouling phenomenon due to the absence of agitation (0 Hz). Considering apparent and real permeabilities, a net differentiation is observed for the highest frequency indicating the necessity to take into account the additional pressure induced by mixing to calculate the accurate driving force (Eq. (7)). However, observation and trends remain similar.

In the literature, several authors had similar observations with PES membranes while filtering red wines. They proposed the adsorption of wine molecules as fouling mechanism [23,24]. Physico-chemical properties of FW may contribute to explain previous observation. El Rayess [25] has measured in FW, the particle size distribution which ranges between 1 and 5 nm. The molecules presents in wine are small compared to the membrane mean pore diameter (0.2 μm). This supports the assumption of fouling mechanisms based on initial pore clogging/adsorption followed by cake formation due to an aggregation of organic matter at the surface of the membrane.

Over FW filtration runs, the water membrane permeabilities were checked with osmotic water. The PES membranes presented a water permeability of $2230 \text{ L h}^{-1} \text{ m}^{-2} \text{ bar}^{-1}$; it is to $281 \text{ L h}^{-1} \text{ m}^{-2} \text{ bar}^{-1}$ for PTFE membranes. These latest values are almost equivalent to final FW permeabilities with a limited gain equal to +28% for PES and +39% for PTFE. All these results indicate that (i) water rinsing and (ii) mechanical stress due to rotational frequency may not remove or reduce fouling propensity and mechanism. It also demonstrates that FW with PES and PTFE membranes generates mainly an irreversible fouling by wine compounds with high fouling intensity due to hydrophobicity (for PTFE membrane).

According to the literature, the mainly compounds contributing

Table 4

Real permeability and hydraulic resistance of membrane along FW filtration.

		L_{p0} [$\text{L h}^{-1} \text{ m}^{-2} \text{ bar}^{-1}$]	L_{p0} [$\text{m s}^{-1} \text{ Pa}^{-1}$]	Rh [$1/\text{m}$]
Water (clean membrane)	PES	4700.0	130×10^{-10}	7.6×10^{10}
	PTFE	2573.0	71.4×10^{-10}	13.9×10^{10}
FW – initial (0 Hz)	PES	3817.2	106×10^{-10}	9.4×10^{10}
	PTFE	3750.3	104×10^{-10}	9.6×10^{10}
FW – final (0 Hz)	PES	1676.3	46.5×10^{-10}	21.4×10^{10}
	PTFE	170.4	4.7×10^{-10}	210×10^{10}
Water-after FW and rinsing	PES	2230.3	6.19×10^{-10}	16.1×10^{10}
	PTFE	281.5	7.81×10^{-10}	127×10^{10}

to the irreversible fouling of membranes are phenolic compounds. Phenolic compounds have more affinity for membrane than polysaccharides [1]. Polyphenol compounds are known as amphiphathic molecules with hydrophobic aromatic rings and hydrophilic phenolic hydroxyl groups. According to Vernhet et al. [26], the adsorption of polyphenols seems to be governed by two mechanisms depending on membrane material: polar interactions (van der Waals interactions and electron donor–acceptor interactions) and hydrogen bonds. The preferential adsorption of phenolic compounds with low polarity membrane suggests the predominance of hydrophobic interactions as in the case of PTFE membranes. Our findings are contradictory with those obtained by Ulbricht et al. [27] who showed that polyphenols are marginally absorbed on low polar membranes and strongly absorbed on high polar membranes.

4.3. RVF filtration of CSW

In a second step, the RVF filtration of CSW is investigated. Fig. 6-A and -B illustrate the evolution of the PES and PTFE membrane permeabilities during the filtration of CSW.

4.3.1. PTFE membranes

For PTFE membranes, a classical and quick decrease of membrane permeability is observed (from $790 \text{ L h}^{-1} \text{ m}^{-2} \text{ bar}^{-1}$ down

to $40 \text{ L h}^{-1} \text{ m}^{-2} \text{ bar}^{-1}$) at the beginning of the filtration ($N=0 \text{ Hz}$). When frequencies of 10 and 20 Hz are applied, a stabilization of permeability is observed at about $25 \text{ L h}^{-1} \text{ m}^{-2} \text{ bar}^{-1}$. For higher frequency at 30 and 40 Hz, a slight permeability increase is reported up to a plateau value (steady-state) of 30 (+20%) and 34 (+36%) $\text{L h}^{-1} \text{ m}^{-2} \text{ bar}^{-1}$ respectively. The permeability values tend to reduce below $25 \text{ L h}^{-1} \text{ m}^{-2} \text{ bar}^{-1}$ if none rotation is applied. Taking into account the additional pressure generated by mixing (real permeability) does not modify the previous described trends.

4.3.2. PES membranes

For PES membranes, membrane permeability decreased quickly (from $260 \text{ L h}^{-1} \text{ m}^{-2} \text{ bar}^{-1}$ down to $22 \text{ L h}^{-1} \text{ m}^{-2} \text{ bar}^{-1}$) at the beginning of the filtration ($N=0 \text{ Hz}$). As previously described with PTFE membranes, the permeability values tend to reduce if none rotation is applied.

Considering filtration up to permeate volume reaches 5 L, the rotational frequencies of 10 Hz did not improve the fluxes (–20% within 30 min). For frequencies equal to 20 Hz, a slight increase in permeability is observed from 18 up to $19.6 \text{ L h}^{-1} \text{ m}^{-2} \text{ bar}^{-1}$ (+9%) within 30 min. When frequency increases, this phenomenon is amplified with permeabilities ranging from 16 up to $26.4 \text{ L h}^{-1} \text{ m}^{-2} \text{ bar}^{-1}$ (+65%) and from 18 up to $72 \text{ L h}^{-1} \text{ m}^{-2} \text{ bar}^{-1}$ (+65%)

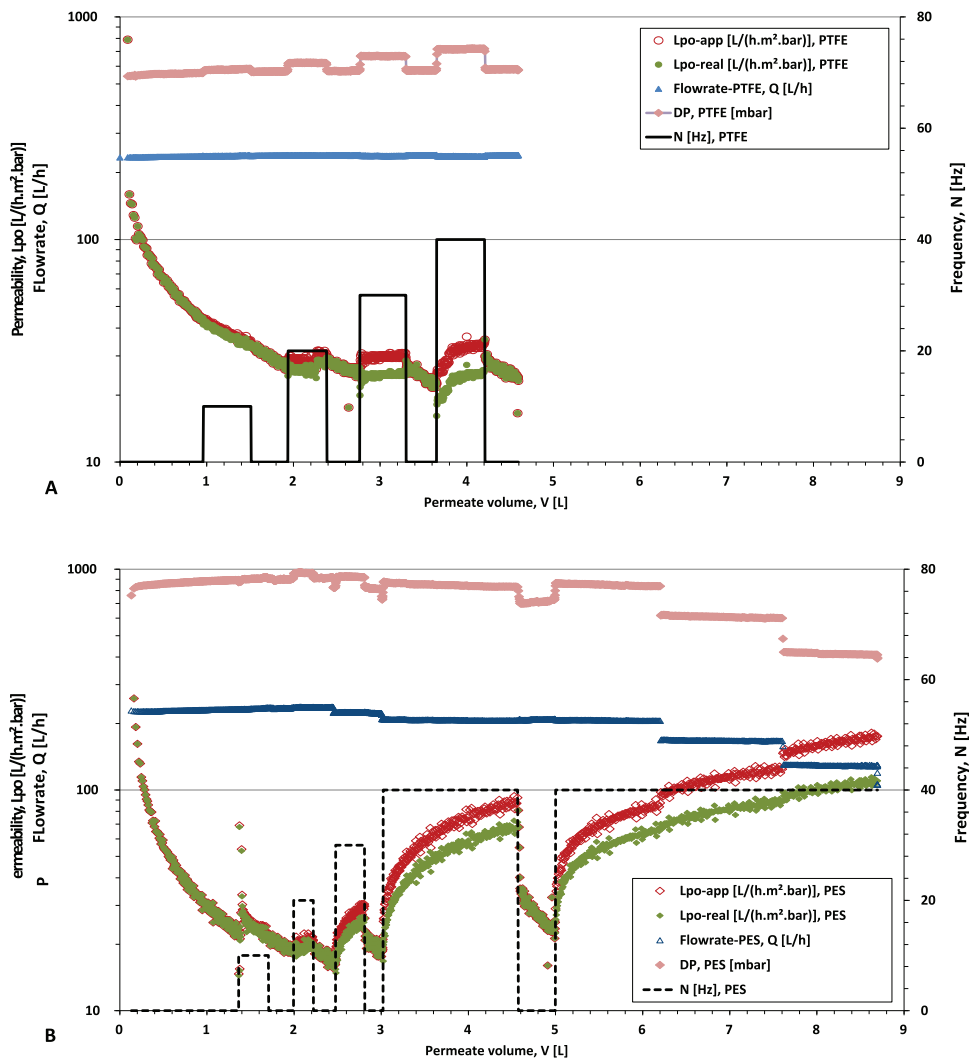


Fig. 6. Evolution of membranes permeabilities of PTFE (A) and PES (B) membranes, flow-rate, DP and N as a function of permeate volume during the RVF filtration ($\Delta P=550$ and 900 mbar, step increase $N=0-40 \text{ Hz}$ alternate with 0 Hz period) of crude simulated wine (CSW).

bar⁻¹ (+300%) respectively for 30 and 40 Hz. For frequencies superior to 20 Hz, the steady-state permeabilities are not achieved indicating fouling removal and flux gain.

Considering this observation, a reduction of driving force (TMP) under 40 Hz was investigated through 3 successive 1 h step (Fig. 6-B from 5 to 9 L). Over this longer period, a significant increase in membrane permeability is observed (from 23 L h⁻¹ m⁻² bar⁻¹ to 105 L h⁻¹ m⁻² bar⁻¹ equivalent to +360%) even if steady-state flux is not established. Apparent and real permeability increases could be attributed to a fouling removal mechanism induced by mechanical effect as previously observed. The continuous increase of real permeability is noticeable whatever TMP. This observation argues for a predominance of mechanical effect of mixing and oscillating movements upon a potential compressibility of cake layer with TMP. In RVF module, velocity and static pressure fields show drastic intensity fluctuation with rotational speed and radial position [28,29]. Filtration performances can be explained by periodic interruption of transmembrane pressure associated to instationarity generation equivalent to pulsed flow. It stands as an original observation but also a promising result for wine clarification.

A comparison between PES and PTFE membrane permeabilities at the initial step (N=0 Hz) indicates that permeability of PTFE membranes is slightly higher than PES membrane (Fig. 6-A and -B). This phenomena is opposite to water permeability of clean membranes equal to 4700 L h⁻¹ m⁻² bar⁻¹ (PES) and 2600 L h⁻¹ m⁻² bar⁻¹ (PTFE) and to permeability during FW filtration runs (initial step, N=0 Hz) respectively for PES and PTFE (1676 and 170 L h⁻¹ m⁻² bar⁻¹). However for CSW, permeability seems to reach a similar threshold around 20 L h⁻¹ m⁻² bar⁻¹ whatever the membrane material without frequency. These observations differ from literature reporting the interest of hydrophobic membranes for crude wine clarification. The experiments conducted on hydrophobic membranes (polypropylene, PP and polyvinylidene difluorure, PVDF) showed them more efficient than hydrophilic membranes for filtration of wines without particles [26].

In present study, when frequency is increased, the performances greatly differ. PES seems to be sensitive to mixing effect (Fig. 6-B) while PTFE seems to be unaffected by the frequency increase (Fig. 6-A) respectively associated with reversible and irreversible fouling contributions. Physicochemical interactions (molecules/membranes and molecules/molecules) seems

dominant with PTFE membrane whereas PES membranes fouling is governed by local hydrodynamics for considered CSW. It seems to indicate that the adsorption and deposition of wine molecules are fostered by the hydrophilic (PES) than by the hydrophobic (PTFE) character of the membrane and generate an irreversible fouling. These results are consistent with those obtained in the literature [1,23,26,27]. When the mixing is stopped, PES membrane permeability decreased sharply and converges slowly towards its long-run value (20 L/h m² bar⁻¹). In such conditions, the permeability of PES membranes may greatly exceed PTFE membranes as demonstrated at 40 Hz. Nevertheless, permeabilities obtained with CSW are almost ten times lower than with FW whatever membrane material.

4.4. Identification of critical frequencies with CSW

According to Fig. 7, the slopes of permeability (dLp₀/dt or dLp₀/dV) were scrutinized as a function of rotational frequency with PES and PTFE membranes during CSW filtration. The reported data correspond to average values during each step. A negative value indicates a fouling kinetics whereas a positive slope informs about cleaning efficiency (fouling removal). The absolute value informs about the propensity of phenomenon.

With FW (Fig. 5), the obtained fluxes remains important. Consequently, RVF filtration is of a limited interest. Permeability kinetics (dLp₀/dt) remains systematically inferior to zero and confirms that the mechanical stress poorly affects the irreversible fouling even under drastic conditions (40 Hz).

With CSW (Fig. 7), both curves, dLp₀/dt and dLp₀/dV as function of frequency, intercept the abscise axe at 21.9/22.8 Hz and 25.8/32.2 Hz, respectively with PES and PTFE membranes. In our conditions, these criteria are named "critical frequencies" and indicate the value above which a permeability increase and hydraulic resistance reduction are observed. The absolute values of kinetics quantify the magnitude of hydraulic resistance/permeability variations which contributes to interpret the balance between reversible and irreversible fouling respectively with PES and PTFE membranes. Irreversible fouling and mechanical effect are much more exacerbated with PES than with PTFE membranes. PES membranes are highly subject to reversible fouling and

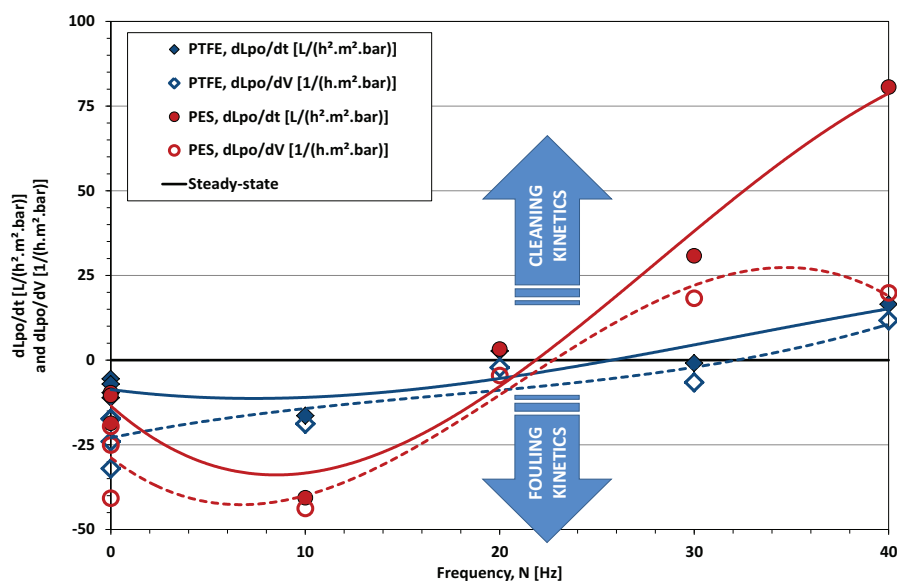


Fig. 7. Evolution of permeability kinetics (dLp₀/dt and dLp₀/dV) of PES and PTFE membranes as a function of frequency during the RVF filtration ($\Delta P=850$ and 570 mbar with PES and PTFE, step increase N=0–40 Hz alternate with 0 Hz period) of crude simulated wine (CSW). Identification of critical frequency determination for dLp₀/dt and dLp₀/dV equal to 0.

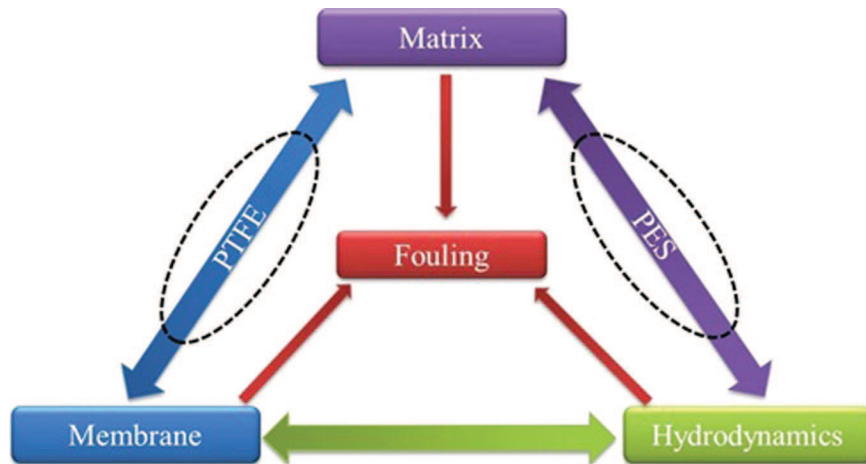


Fig. 8. Factors influencing the fouling of PES and PTFE membranes.

mechanical impact of RVF module is highly efficient whereas PTFE membranes are mainly affected by irreversible fouling. Under accurate operating conditions (CSW, $N=40$ Hz), the present results contribute to understand why hydrophilic PES membranes exhibit higher performances than hydrophobic PTFE membranes. Consequently, critical working conditions (frequencies) depend on interactions between membrane materials and wine composition.

5. Conclusion

A shear enhanced process called Rotating and Vibrating Filtration (RVF technology) was investigated for the clarification of filtered wine and crude simulated wine. The impact of membrane material (hydrophilic PES and hydrophobic PTFE materials with a cut-off equal to $0.2 \mu\text{m}$), wine composition (filtered wine, FW and crude simulated wine, CSW) and operating conditions (transmembrane pressure and rotational frequency) were reported.

For FW, the irreversible fouling is dominant and consequently the mechanical impact of RVF is limited. The permeability of PES membrane is superior to PTFE one but in both cases a high fluxes could be obtained ($> 1000 \text{ L h}^{-1} \text{ m}^{-2}$) under standard operating conditions. None momentum nor mass transfer limitations appear as a critical bottleneck so that RVF filtration seem not to be an accurate technology in such case. Basically, the product is easy enough to filter with standard technology such as dead-end and crossflow microfiltration.

For CSW, a more complex balance between reversible and irreversible fouling is observed with PES and PTFE membranes. A strong mechanical effect with PES membrane whereas a moderated one with PTFE membrane is noticeable. The relative propensity of irreversible and reversible fouling is membrane/matrices dependant. The RVF technique is particularly interesting because fouling control is operated without back-flushing and permeate loss.

Factors affecting the fouling of the two membranes are summarized in Fig. 8 where the PTFE membrane fouling seems to be greatly affected by the molecules/membrane interactions and the PES membrane fouling rather affected by a balance between the hydrodynamics of the system and the deposited material.

Our study strategy leads to highlight and to demonstrate that the mechanical impact can constitute the lever arm to significantly increase the hydraulic performances through a correlation between its intensity and the permeability gain. Moreover, the critical frequencies were defined and determined which help to characterize and to rank the complex "membrane-fluid" interactions.

Future scientific works will investigate the local hydrodynamics within RVF module in order to explain these good performances.

Moreover in such complex mechanical and hydrodynamics device, the scale-up constitutes real technical and scientific challenges for which this local information is determinant.

Nomenclature

J	flux ($\text{L h}^{-1} \text{ m}^{-2}$)
μ	viscosity (Pa s)
D	diameter (m)
$\Delta\Pi$	transmembrane pressure (Pa)
$\Delta\Pi_{\alpha\gamma}$	local additional pressure
Hz	hertz
k	core velocity coefficient
L_p	permeability ($\text{L h}^{-1} \text{ m}^{-2} \text{ bar}^{-1}$)
N	rotation Frequency (Hz)
PP	permeate pressure (bar)
PR	retentate pressure (bar)
Q	flowrate (L h^{-1})
ρ	density (kg m^{-3})
r	radius (m)
S	filtration area (m^2)
$\Delta\bar{P}_{ag}$	average additional transmembrane pressure (Pa)
CFMF	crossflow microfiltration
CSW	crude simulated wine
FW	filtered wine
CI	Color Intensity
TPI	Total Polyphenol Index
NTU	Nephelometric Turbidity Unit
OD	optical density
PES	polyethersulfone
PTFE	polytetrafluoroethylene
RVF	Rotating and Vibrating Filtration
TMP	driving force
VRR	volume reduction ratio

References

- [1] Y. El Rayess, C. Albasi, P. Bacchin, P. Taillandier, J. Raynal, M. Mietton-Peuchot, A. Devatine, Cross-flow microfiltration applied to oenology: a review, *J. Membr. Sci.* 382 (2011) 1–19.
- [2] Y. El Rayess, C. Albasi, P. Bacchin, P. Taillandier, J. Raynal, M. Mietton-Peuchot, A. Devatine, Analysis of membrane fouling during cross-flow microfiltration of wine, *Innov. Food Sci. Emerg. Technol.* 16 (2012) 398–408.

- [3] B. Boissier, F. Lutin, M. Moutounet, A. Vernhet, Particles deposition during the cross-flow microfiltration of red wines-incidence of the hydrodynamic conditions and of the yeast to fines ratio, *Chem. Eng. Process.* 47 (2008) 276–286.
- [4] Y. El Rayess, C. Albasi, P. Bacchin, P. Taillandier, J. Raynal, M. Mietton-Peuchot, A. Devatine, Cross-flow microfiltration of wine: effect of colloids on critical fouling conditions, *J. Membr. Sci.* 385 (2011) 177–186.
- [5] Y. Bessiere, N. Abidine, P. Bacchin, Low fouling conditions in dead-end filtration: evidence for a critical filtered volume and interpretation using critical osmotic pressure, *J. Membr. Sci.* 264 (2005) 37–47.
- [6] M.Y. Jaffrin, Dynamic filtration with rotating disks, and rotating and vibrating membranes: an update, *Curr. Opin. Chem. Eng.* 1 (2012) 171–177.
- [7] M.Y. Jaffrin, Dynamic shear-enhanced membrane filtration: a review of rotating disks, rotating membranes and vibrating systems, *J. Membr. Sci.* 324 (2008) 7–25.
- [8] C. Harscoat, M.Y. Jaffrin, R. Bouzerar, J. Courtois, Influence of fermentation conditions and microfiltration processes on membrane fouling during recovery of glucuronane polysaccharides from fermentation broths, *Biotechnol. Bioeng.* 65 (1999) 500–511.
- [9] A. Brou, L. Ding, P. Boulnois, M.Y. Jaffrin, Dynamic microfiltration of yeast suspensions using rotating disks equipped with vanes, *J. Membr. Sci.* 197 (2002) 269–282.
- [10] L.H. Ding, O. Akoum, A. Abraham, M.Y. Jaffrin, High shear skim milk ultrafiltration using rotating disk filtration systems, *AIChE J.* 49 (2003) 2433–2441.
- [11] O. Akoum, M.Y. Jaffrin, L.H. Ding, Concentration of total milk proteins by high shear ultrafiltration in a vibrating membrane module, *J. Membr. Sci.* 247 (1) (2005) 211–220.
- [12] M. Frappart, O. Akoum, L.H. Ding, M.Y. Jaffrin, Treatment of dairy process waters modelled by diluted milk using dynamic nanofiltration with a rotating disk module, *J. Membr. Sci.* 282 (1) (2006) 465–472.
- [13] L. Fillaudeau, B. Boissier, A. Moreau, P. Blanpain-Avet, S. Ermolaev, N. Jitariouk, A. Gourdon, Investigation of rotating and vibrating filtration for clarification of rough beer, *J. Food Eng.* 80 (1) (2007) 206–217.
- [14] V. Espina, M.Y. Jaffrin, L. Ding, B. Cancino, Fractionation of pasteurized skim milk proteins by dynamic filtration, *Food Res. Int.* 43 (5) (2010) 1335–1346.
- [15] Z. Zhu, J. Luo, L. Ding, O. Bals, M.Y. Jaffrin, E. Vorobiev, Chicory juice clarification by membrane filtration using rotating disk module, *J. Food Eng.* 115 (2) (2013) 264–271.
- [16] C. Nurra, C. Torras, E. Clavero, S. Rios, M. Rey, E. Lorente, X. Farriol, J. Salvado, Biorefinery concept in a microalgae pilot plant. Culturing, dynamic filtration and steam explosion fractionation, *Bioresour. Technol.* 163 (2014) 136–142.
- [17] Y. El Rayess, M. Mietton-Peuchot, Integrated membrane processes in wine-making, in: A. Cassano, E. Drioli (Eds.), *Integrated Membrane Operations in the Food Production*, 1st ed., De Gruyter, Germany, 2014.
- [18] L. Fillaudeau, B. Boissier, S. Ermolaev, N. Jitariouk, A. Gourdon, Etude hydrodynamique d'un module de filtration dynamique pour fluides alimentaires, *Ind. Alim. Agr.* 124 (2007) 8–16.
- [19] R. Bouzerar, M.Y. Jaffrin, L. Ding, P. Pautier, Influence of geometry and angular velocity on performance of a rotating disk filter, *AIChE J.* 46 (2000) 257–265.
- [20] R. Bouzerar, L. Ding, M.Y. Jaffrin, Local permeate flux-shear-pressure relationships in a rotating disk microfiltration module: implications for global performances, *J. Membr. Sci.* 170 (2000) 127–141.
- [21] M.Y. Jaffrin, L.H. Ding, O. Akoum, A. Brou, A hydrodynamic comparison between rotating disk and vibratory dynamic filtration systems, *J. Membr. Sci.* 242 (2004) 155–167.
- [22] P. Ribéreau-Gayon, Y. Glories, A. Maujean, D. Dubourdieu, *Handbook of Enology Volume 2 : The Chemistry of Wine, Stabilization and Treatments*, 2nd ed., Dunod, Paris, 2006.
- [23] A. Vernhet, M. Moutounet, Fouling of organic microfiltration membranes by wine constituents: importance, relative impact of wine polysaccharides and polyphenols and incidence of membrane properties, *J. Membr. Sci.* 201 (2002) 103–122.
- [24] A. Vernhet, D. Cartalade, M. Moutounet, Contribution to the understanding of fouling build-up during microfiltration of wines, *J. Membr. Sci.* 211 (2003) 357–370.
- [25] Y. El Rayess, *Microfiltration tangentielle appliquée à l'oenologie: compréhension et maîtrise des phénomènes de colmatage* (Ph.D. thesis), University of Toulouse, 2011.
- [26] A. Vernhet, M.N. BellonFontaine, J.M. Brillouet, E. Roesink, M. Moutounet, Wetting properties of microfiltration membrane: determination by means of the capillary rise technique and incidence on the adsorption of wine polysaccharide and tannins, *J. Membr. Sci.* 128 (1997) 163–174.
- [27] M. Ulbricht, W. Ansoerge, I. Danielzik, M. Konig, O. Schuster, Fouling in microfiltration of wine: the influence of the membrane polymer on adsorption of polyphenols and polysaccharides, *Sep. Purif. Technol.* 68 (2009) 335–342.
- [28] M. D'Esparbes, Ph. Schmitz, L. Fillaudeau, CFD and experimental approaches to investigate a dynamic filtration module for bio- and food-processes, *Récents Progrès en Génie des Procédés*, Numéro 101 – 2011, ISSN 1775-335X - ISBN 2-910239-75-6, Ed. SFGP, Paris, France.
- [29] X. Xie, Ph. Schmitz, N. Dietrich, L. Fillaudeau, Investigation of velocity field (by particle image velocimetry) in turbulent flow regime within a dynamic filtration module, in: *Proceedings of ECCE10*, September 2015.